

**DEW AND FROST DEPOSITION AND THEIR ROLE IN THE REGULATION OF
RADIATION FOG ONSET: A NUMERICAL SENSITIVITY STUDY**

Robert Tardif

Program in Atmospheric and Oceanic Sciences
University of Colorado at Boulder

*Term paper for
ATOC 5225 Thermodynamics of Atmospheres and Oceans*

December 2001

Program in Atmospheric and Oceanic Sciences
University of Colorado at Boulder
Duane Physics
Campus Box 311
Boulder, Colorado, 80309-0311

ABSTRACT

The deposition of dew or frost on elements at the ground surface leads to a water vapor depletion in the few lowest meters of the boundary layer. This loss of water vapor, hence reduction in relative humidity, can have an impact on the time of fog onset, possibly even preventing the formation of fog.

The importance of dew deposition upon the formation of radiation fog is assessed using a one-dimensional boundary layer model. Also, the dependence of dew deposition rates upon geostrophic wind speed is evaluated through numerical simulations. Results suggest that the use of a proper parameterization of dew / frost deposition at the surface is necessary for accurate numerical prediction of radiation fog events.

1. Introduction

The onset of a radiation fog occurs under the influence of isobaric cooling near the ground due to radiative flux divergence. This usually happens after sunset under clear skies, as the divergence of longwave radiation is a maximum under these conditions. If the cooling is enough to lower the temperature to the dew point temperature, then fog appears. This simplistic description assumes there is enough cloud condensation nuclei (CCN) in the air near the surface so that fog droplets are activated at low supersaturations.

Generally speaking, the relative humidity can be increased by lowering the temperature or by adding water vapor to the system. Inversely, if some water vapor is taken out of the system or if its temperature is increased, a decrease in relative humidity occurs. Also, an increase or decrease in relative humidity can occur as a result of mixing two air masses. Processes regulating the evolution of the near surface relative humidity determine if a fog layer will form or not. One of these processes is the loss of water vapor in the surface layer by the deposition of atmospheric water as dew on surface elements. It should be noted that dew, as it is observed (condensed water on surface elements), actually arises from two sources. The condensed water forming dew on a vegetation canopy may come from the atmosphere (deposition or sometimes referred to as dewfall) or from an upward flux of vapor from the soil to the canopy (distillation) (Monteith, 1957). For a bare soil surface, the dewfall dominates. Here we focus only on the atmospheric contribution (dewfall), as it is the process controlling the atmospheric relative humidity and thus the onset of fog.

During the evening transition of the boundary layer (BL), the near surface relative humidity (RH) evolution is determined by the opposing effects of cooling (increase of RH) and of dew deposition (decrease of RH). Dew deposition at the surface occurs as the ground surface cools so that the saturation specific humidity at the ground temperature ($q_{\text{sat}}(T_{\text{sfc}})$) becomes lower than the water vapor specific humidity of the moist air in contact with the surface ($q_{\text{air}}(z=0)$):

$$q_{air}(z = 0) > q_{sat}(T_{sfc}). \quad (1)$$

If the surface temperature is below 0°C, frost deposition occurs instead of dew. Also, dew (or frost) may form when moist air aloft is brought to the surface by turbulent eddies. If this air is moist enough and the surface temperature is low enough, condensation on elements at the surface is observed. It is believed that dew deposition related to intermittent turbulent eddies in the stably stratified nocturnal boundary layer enhances the rate at which dew forms on the surface. In fact, since molecular diffusion is small in the atmosphere, the turbulent diffusion should dominate. But the intensity of the turbulence must remain somewhat weak in order to observe dew formation at the surface. Strong turbulent mixing near the surface during the evening transition will result in a less important cooling rate as warm air above the inversion is mixed with the cooler surface air. Then the surface specific humidity may not reach its saturation value. So, it is speculated that there exist a critical threshold for turbulence intensity in determining the occurrence of dew formation, depending on the amount of moisture in the air. But the study of this threshold is beyond the scope of this paper.

Previous studies have pointed out the role dew deposition plays in “controlling” the onset of fog layers (Lala et al., 1975 a, b; Brown and Roach, 1976 and Pickering and Jiusto, 1978). For a given radiative cooling rate, if the loss of moisture to the surface is large enough, fog formation may be inhibited. Wattle et al. (1984) report measured dew deposition rates as large as 20 gm²hr⁻¹ during pre-fog periods during the FOG-82 field experiment. Such rates lead to some dehydration of the lower surface layer. Pilié et al. (1975a, b) points out that dew deposition is responsible for the formation of a near-surface dew point inversion. The formation of this inversion is thought to be the mechanism responsible for the initial formation of fog aloft, in opposition to ground fog.

Bergot and Guédalia (1994) performed a sensitivity study on time of dense fog formation to dew deposition using a one-dimensional model. In their experiments, results show the effect of dew deposition can delay the fog formation by 4 hours. They also assessed the variability of total dew deposition to geostrophic wind speed. The horizontal

pressure force (geostrophic wind) determines the wind shear near the surface and thus the frequency and intensity of turbulent events or bursts in the stable surface layer. They showed that an increase in geostrophic wind speed from 2 ms^{-1} to 10 ms^{-1} increased the total amount of dew deposition from about 15 gm^{-2} to 150 gm^{-2} .

The present paper describes results from a numerical sensitivity study similar to the one discussed in Bergot and Guédalia (1994) but goes into a more detailed analysis of dew and frost deposition rates and their impact on fog formation. In section 2, the model used is briefly described, while the numerical experiments performed are described in section 3. Results are presented in section 4 and conclusions are outlined in section 5.

2. Model description

The COBEL (**CO**uche **B**rouillard **E**au **L**iquide) high-resolution one-dimensional boundary layer model is used for the study. The code used is in fact a more recent version of the model used by Bergot and Guédalia (1994). This model was originally developed at the Laboratoire d'Aérodologie, Université Paul Sabatier, France to study physical processes in the strongly stratified nocturnal boundary layer (Estournel and Guédalia, 1987). It has since been adapted to real-time forecasting of dense fog events (Bergot, 1993, Peyraud, 2001) and more recently stratus cloud layers (Tardif, 2000). Using a high-resolution model adapted to the nocturnal boundary layer is necessary in the present context. Indeed, important stratification in the temperature and humidity profiles is observed over thin layers within the nocturnal BL. These gradients need to be resolved in order to accurately represent the soil-atmosphere exchanges of heat and moisture.

Here, only a general description of the overall characteristics of the model is given. A more detailed description is given of the parameterization of soil-atmosphere interactions. The reader is referred to the Appendix for a more detailed description of other model components.

a. General description

The model's dynamical and thermodynamical equations are derived from the ensemble-average Boussinesq equations. Horizontal homogeneity of momentum and of turbulent fluctuations is assumed, but non-homogeneities in the large-scale temperature and humidity fields are considered (horizontal advections), as well as large-scale vertical motion. The model's prognostic variables are the horizontal wind components, potential temperature, specific humidity and liquid water content. An additional prognostic equation for turbulence kinetic energy is used as part of the turbulent mixing parameterization (1.5 order closure). Radiation is taken into account by using a high spectral resolution (232 channels) radiative transfer scheme in the infrared (IR) part of the spectrum (Vehil et al., 1989), and a simpler monospectral parameterization for the shortwave radiation (Fouquart and Bonnel, 1980). Condensation is represented with an "all or nothing" condensation scheme, in which condensation of fog droplets occur whenever the relative humidity goes above 100%. This representation assumes there is a sufficient amount of cloud condensation nuclei (CCN) so that condensation occurs at low levels of supersaturation. Computations are performed on a high vertical resolution grid, composed of 30 levels distributed between the ground and an altitude of about 1.5 km using a log-linear function. The lowest model level in the atmosphere is at 0.5 m, the second lowest is at 1.65m etc. Efficient numerical methods are used to solve the equations to ensure stability of the solutions (see Appendix).

b. Soil-atmosphere coupling

Thermal coupling as well as exchanges of water vapor between the surface and the atmosphere is performed through the surface energy budget equation:

$$\left(F_{IR} \downarrow - \varepsilon_s \sigma T_{so}^4 \right) + (1 - \alpha_s) F_{vis} \downarrow + H + (L \cdot E) + G = 0 \quad (2)$$

where T_{so} is the surface skin temperature. The first term is the net longwave radiation at the surface while the second is the net shortwave radiation (α_s is the surface albedo). H is

the surface sensible heat flux, (L·E) the surface latent heat flux and G is the heat flux into the ground. H and G are determined following:

$$H = \rho c_p \left(K \frac{\partial T}{\partial z} \right) \Big|_{z=0} \quad (3)$$

$$G = -K_s \left(\frac{\partial T_s}{\partial z} \right) \Big|_{z=0}, \quad (4)$$

while the water vapor flux at the surface is expressed as (Noilhan and Planton, 1989):

$$E = \rho C_h (q_{z1} - Hu \cdot q_{sat}(T_{so})), \quad (5)$$

where q_{z1} is the specific humidity at the lowest model level in the atmosphere, $q_{sat}(T_{so})$ the saturation specific humidity at the surface temperature, C_h an exchange coefficient and Hu is the surface relative humidity. Hu is taken to be a function of soil volumetric water content W following Mihailovic *et al.* (1993) :

$$Hu = \begin{cases} 1.0 - \left(\frac{W_{\max} - W_{\text{superficial}}}{W_{\max}} \right)^3 & W_{\text{superficial}} < W_{\max} \\ 1.0 & W_{\text{superficial}} \geq W_{\max} \end{cases} \quad (6)$$

$W_{\text{superficial}}$ is the volumetric soil water content in the near surface superficial layer and W_{\max} is the field capacity i.e. maximum water content the soil can hold before surface storage (ponding) occurs. It can be pointed out that this surface evaporation formulation does not take into account the contribution from evapotranspiration of vegetation. The exchange coefficient C_h is expressed as (Pielke, 1984, p.153):

$$C_h = \frac{ku^*}{0.74 \left(\ln \left(\frac{z}{z_o} \right) + 6.35 \frac{z}{L_{mo}} \right)}, \quad (7)$$

where L_{mo} is the surface layer Monin-Obukhov length, u^* the friction velocity and z_o the roughness length. The friction velocity is computed following the K-closure technique:

$$u^* = K_m^{1/2} \left(\left(\frac{\partial u}{\partial z} \right)^2 + \left(\frac{\partial v}{\partial z} \right)^2 \right)^{1/4}, \quad (8)$$

where K_m is evaluated with (A.8) (see Appendix).

When the temperature becomes lower than the freezing point, frost deposition occurs instead of dew deposition. To represent this effect, the considered saturation specific humidity is modified since differences in saturation vapor pressures over ice and water indicate that the deposition of frost can be more important than the deposition of dew. This modified saturation specific humidity is taken to be:

$$q_{sat\ frost}(T_{so}) = q_{sat}(T_{so}) \frac{e_{is}(T_{so})}{e_{ws}(T_{so})}, \quad (9)$$

where $e_{is}(T_{so})$ is the saturation vapor pressure over ice and $e_{ws}(T_{so})$ is the saturation vapor pressure over water.

The evolution of both soil temperature and soil moisture needs to be represented for accurate prediction of BL temperature and humidity. Within COBEL, soil temperature (T_s) evolution is represented through the diffusion equation:

$$\frac{\partial T_s}{\partial t} = \frac{\partial}{\partial z} \left(\frac{K_s}{\rho_s C_{ps}} \frac{\partial T_s}{\partial z} \right), \quad (10)$$

where K_s is the thermal conductivity, ρ_s the volumetric mass and C_{ps} is the specific heat of the soil. Thermal conductivity is a highly non-linear function of soil moisture.

Soil moisture evolution is computed using the soil model of Mahrt and Pan (1984). This model does not account for horizontal variations of soil type or conditions. The grid used consists of a thin superficial layer (5 cm) near the surface and a thicker lower layer of 95 cm thick. The non-dimensional volumetric soil water content (W) evolution is expressed as:

$$\frac{\partial W}{\partial t} = \frac{\partial}{\partial z} \left[D(W) \frac{\partial W}{\partial z} \right] + \frac{\partial K(W)}{\partial z}, \quad (11)$$

where $D(W)$ is the hydraulic diffusivity and $K(W)$ the hydraulic conductivity. Both parameters are soil type dependent and can vary by several orders of magnitude from dry to wet soil conditions.

3. Experiments

Numerical experiments are performed to illustrate the importance dew deposition has on controlling the formation of fog layers. Parameters thought to be most important in determining the amount of vapor condensing as dew are perturbed and results are compared. Comparisons are based on the formation or non-formation of a fog layer during short-term simulations, along with dew deposition amount and instantaneous dew deposition rates.

The numerical experiments performed are based on the conditions observed in the north of France on the evening of November 6 1988. The observations were taken at an instrumented site in the Carnin commune near Lille, as part of the Lille88 fog field experiment (Guédalia and Bergot, 1992). The surface is characterized by a homogeneous bare soil (wintertime plowed fields). On the chosen day, a sounding taken at 1500 UTC (an hour before sunset) indicate a stable moist boundary layer with a mean specific humidity of about 4 gkg^{-1} (Fig. 1). The relative humidity in the boundary layer is about 70%. Under clear sky and light wind conditions these profiles are conducive to the

formation of a dense fog layer during the night. All numerical experiments presented here are performed using these initial conditions.

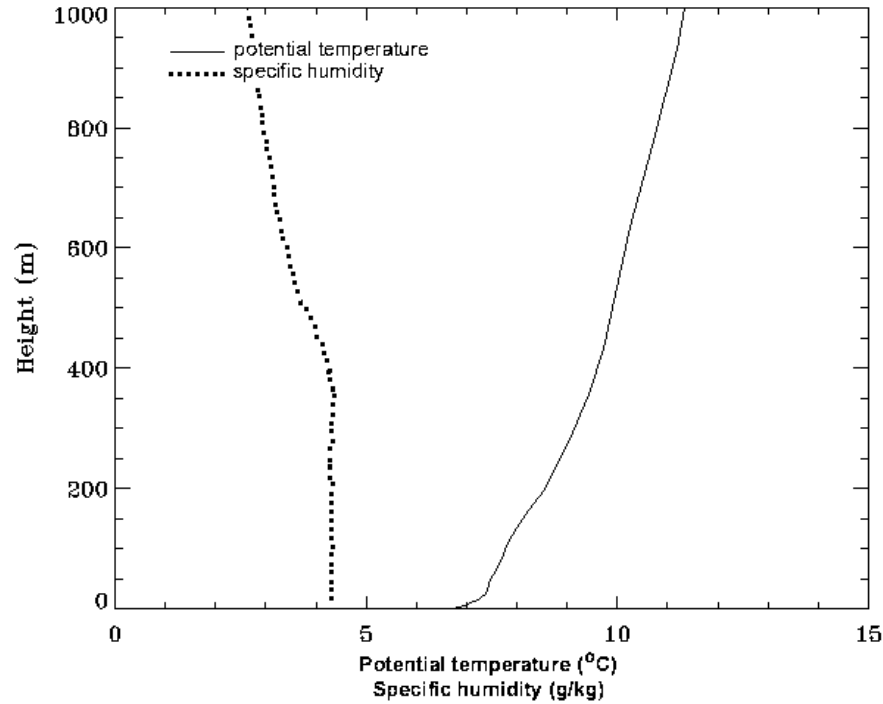


Fig. 1. Profiles of potential temperature and specific humidity used as initial conditions for the numerical experiments.

Based on wind measurements at the site, the geostrophic wind speed is deduced to be about 2 ms^{-1} in the lower atmosphere. Consequently, a baseline simulation is performed using this value and the initial profiles described above. For this baseline simulation, all other external forcings (temperature and humidity horizontal advections, vertical motion) are set to zero. The initial wind profile used is specified in order to be consistent with the pressure force (geostrophic wind). The initial wind speed is taken to be geostrophic above 100m and decreasing exponentially toward a small value close to the surface. This profile is consistent with the observed profile shown in Bergot (1993).

First, a set of experiments is performed to assess the role of turbulent mixing intensity in determining the amount of dew deposition at the surface. Simulations are performed with geostrophic wind speed values of 1, 2 and 4 ms^{-1} . This corresponds to

taking the baseline value of 2 ms^{-1} and dividing/multiplying it by a factor of 2 to decrease/increase the level of shear induced turbulent mixing near the ground.

To illustrate the sensitivity of the formation of a fog layer upon the amount of vapor lost to the surface as dew, a simulation is performed while the dew deposition is switched off altogether. This is equivalent to forcing the exchange coefficient C_h in equation (5) to be zero whenever a downward vapor flux to the surface is detected during the model simulation. The experiment is referred as the “no dew/no frost” experiment.

Another experiment is performed while dew deposition is taken into account, but without the correction that should be applied when frost deposition occurs. In other words, even if the surface temperature goes below 0°C , the e_{is}/e_{ws} term in equation (9) is taken to be equal to 1. This is referred as the “no frost” experiment.

4. Results

a. Baseline simulation

The baseline simulation (full model physics + initial conditions described in the previous section + geostrophic wind speed equal to 2 ms^{-1}) shows the onset of a fog layer at 1700 UTC (Fig. 2). The fog layer grows in the vertical up to 25 m at the end of the 9-hour integration and becomes denser with time as shown by the decrease of the horizontal visibility (Fig. 3). These results are consistent with those obtained by Guédalia and Bergot (1994).

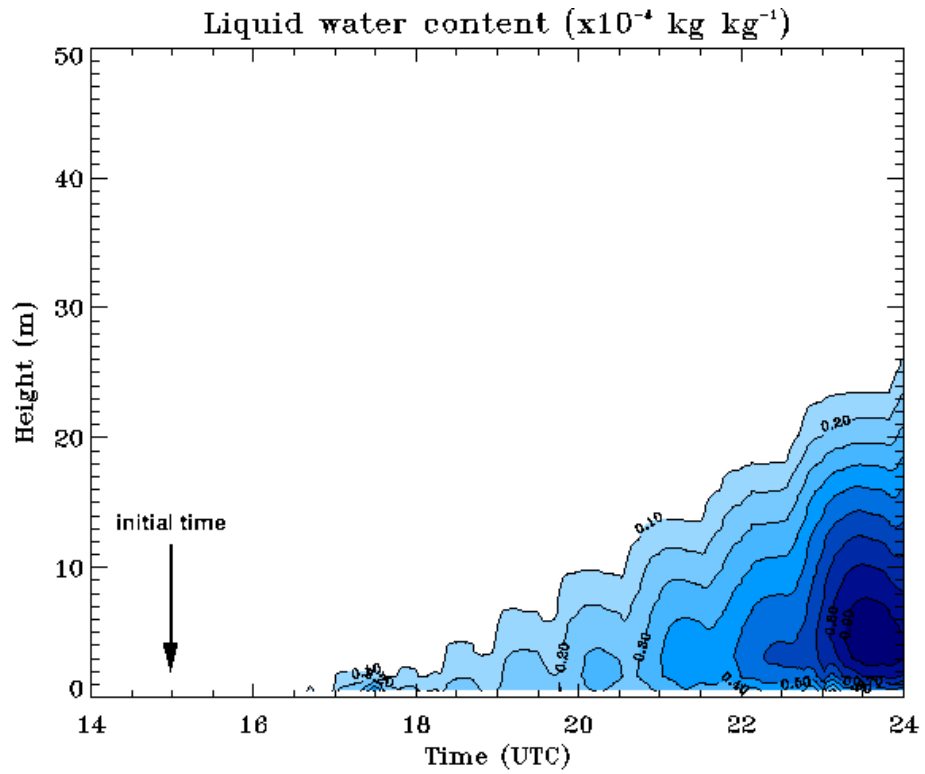


Fig. 2. Time-height cross-section of liquid water content for the baseline simulation. Fog water content contours are shown at every 0.1 gkg^{-1} . The maximum water content shown is 0.9 gkg^{-1} .

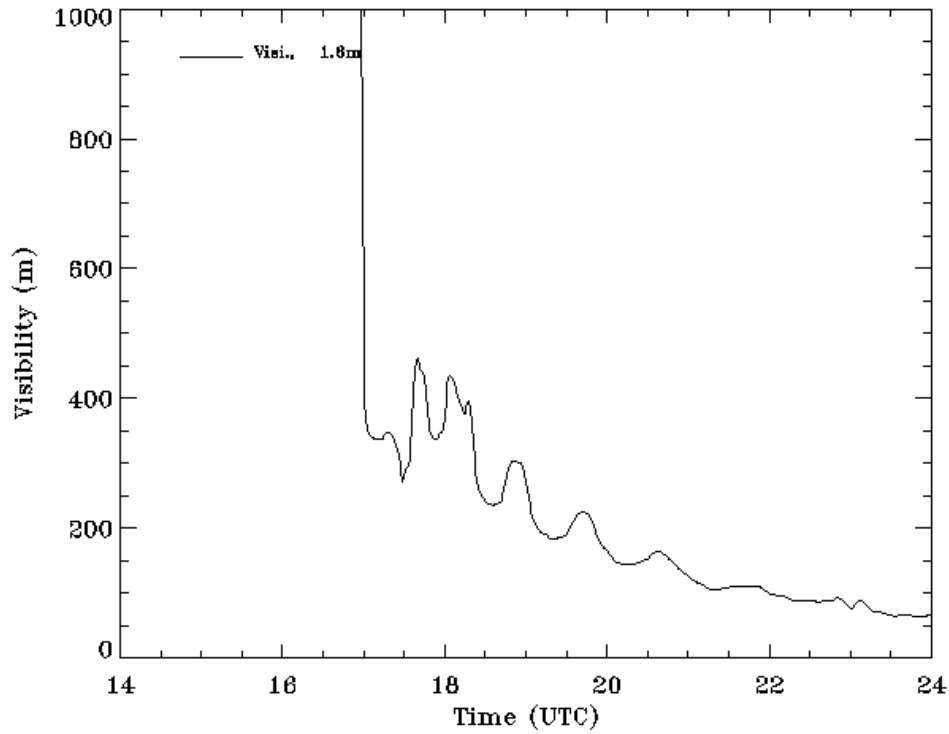


Fig. 3. Temporal evolution of the simulated horizontal visibility at 1.65 m for the baseline simulation ($|V_g| = 2 \text{ ms}^{-1}$).

b. Sensitivity to geostrophic wind speed

Similar simulations were performed with different values of the geostrophic wind speed ($|V_g|$). Results obtained with $|V_g| = 1 \text{ ms}^{-1}$ show the onset of a fog layer at 1700 UTC and a fog depth of 25 m at the end of the simulation. These results are identical to the baseline simulation. The main difference is the maximum water content at the end of the simulation. A higher water content is obtained, with a value above 1 gkg^{-1} observed in the lowest 10 m at 2400 UTC, compared to a content slightly above 0.9 gkg^{-1} for the baseline simulation. This lower water content may be related to decreased mixing with the air above the inversion or to a lower dewfall rate.

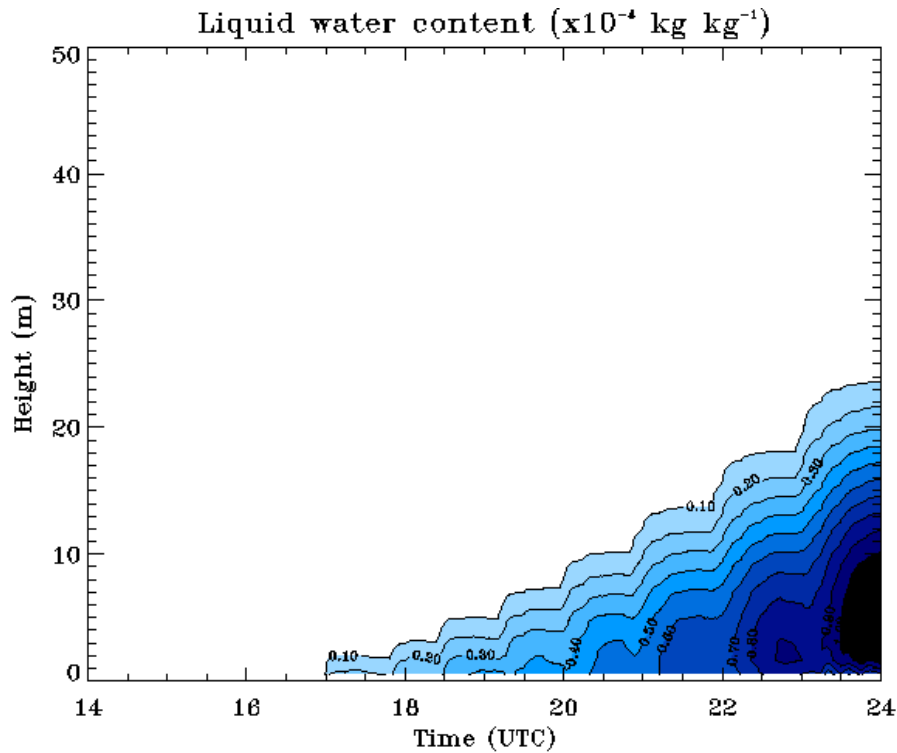


Fig. 4. Time-height cross-section of liquid water content for the simulation performed with $|V_g| = 1 \text{ ms}^{-1}$. Fog water content contours are shown at every 0.1 gkg^{-1} . The maximum water content shown is 1.0 gkg^{-1} .

For a simulation performed with a geostrophic wind speed of 4 ms^{-1} , no fog layer formed during the 9-hour simulation.

To assess if observed differences are related to an increase of water vapor depletion due to dew deposition, the integrated (cumulative) amount of water condensed at the surface (dew deposition) is compared for the three simulations (Fig. 5). Results show the amount of vapor condensed as dew on the surface is indeed strongly dependent on the intensity of turbulent mixing close to the surface, as driven by the magnitude of the geostrophic wind speed.

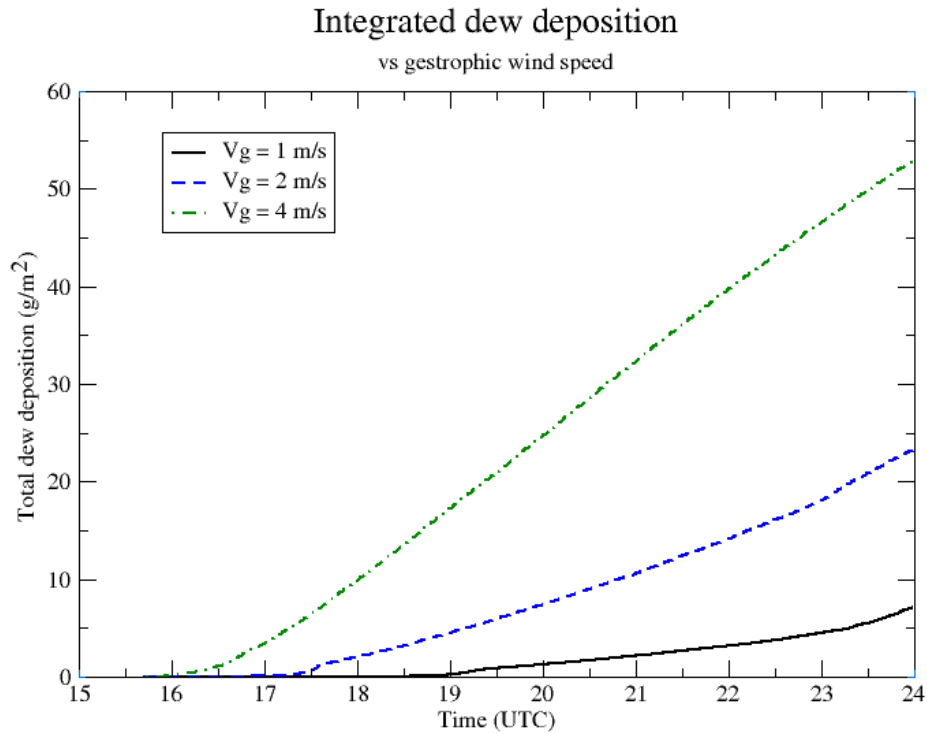


Fig. 5. Temporal evolution of the total (integrated) amount of water vapor condensed as dew on the surface obtained using various geostrophic wind speeds.

Results show the amount of dewfall increases with geostrophic wind speed, from 7 gm^{-2} for $|V_g| = 1 \text{ ms}^{-1}$ to 23 gm^{-2} for $|V_g| = 2 \text{ ms}^{-1}$ and to 53 gm^{-2} for $|V_g| = 4 \text{ ms}^{-1}$ after 9 hours of model integration. Also, it is observed that significant amount of dew deposition is initiated earlier for stronger geostrophic wind speeds. Figure 6 shows the simulated temporal evolution of instantaneous dew deposition rates (in gh^{-1}). As expected, the rate at which dewfall occurs is higher for larger geostrophic wind speeds. This is verified for the entire length of the simulations. Table I shows average values and standard deviation of dew deposition rates for the three simulations. Values are computed using model output at every time steps and for the entire length of the simulations. Increasing the geostrophic wind speed from 1 to 2 ms^{-1} increases the average dew deposition rate by a factor of 3, while an increase from 2 to 4 ms^{-1} leads to an increase by a factor of 2. It should be noted that the dewfall values obtained in this study are consistent with values

reported by Pickering and Justo (1978), Wattle et al. (1984) and Garratt and Segal (1988).

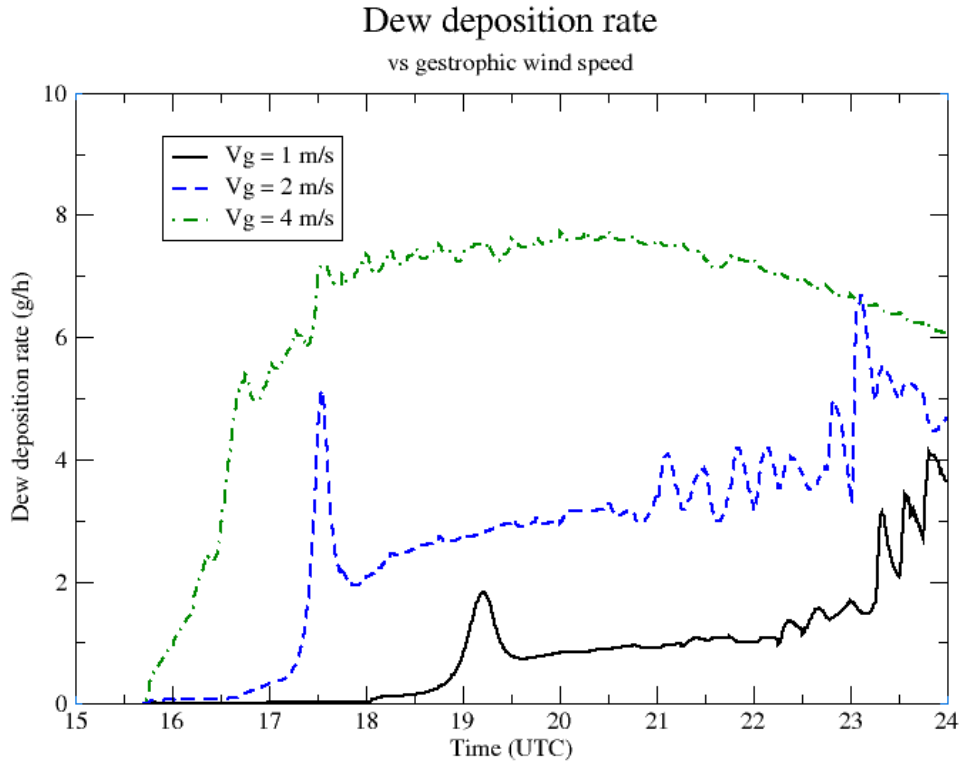


Fig. 6. Temporal variations of the instantaneous rates of dew deposition obtained using different values of geostrophic wind speeds.

TABLE I
Average and standard deviation of instantaneous dew deposition rates for various values of geostrophic wind speeds.

Geostrophic wind speed (ms^{-1})	Average instantaneous dew deposition rate ($\text{gm}^{-2}\text{h}^{-1}$)	Standard deviation ($\text{gm}^{-2}\text{h}^{-1}$)
1.0	0.93	0.90
2.0	2.97	1.47
4.0	6.54	1.56

c. 'no dew/no frost' and 'no frost' experiments

Two other model simulations were performed to illustrate the role dew/frost deposition plays in controlling the onset of a fog layer. Using the same initial conditions as before, and using a geostrophic wind speed of 4 ms^{-1} , simulations were performed while disabling the dew/frost deposition altogether (imposing a zero value throughout the simulation). The reader is reminded that *with dew deposition*, a similar simulation didn't result in the formation of a fog layer. Without any dew or frost deposition at the surface, a shallow fog layer forms at 1600 UTC with a water content of about 0.8 gkg^{-1} forming rapidly near the ground (Fig. 7).

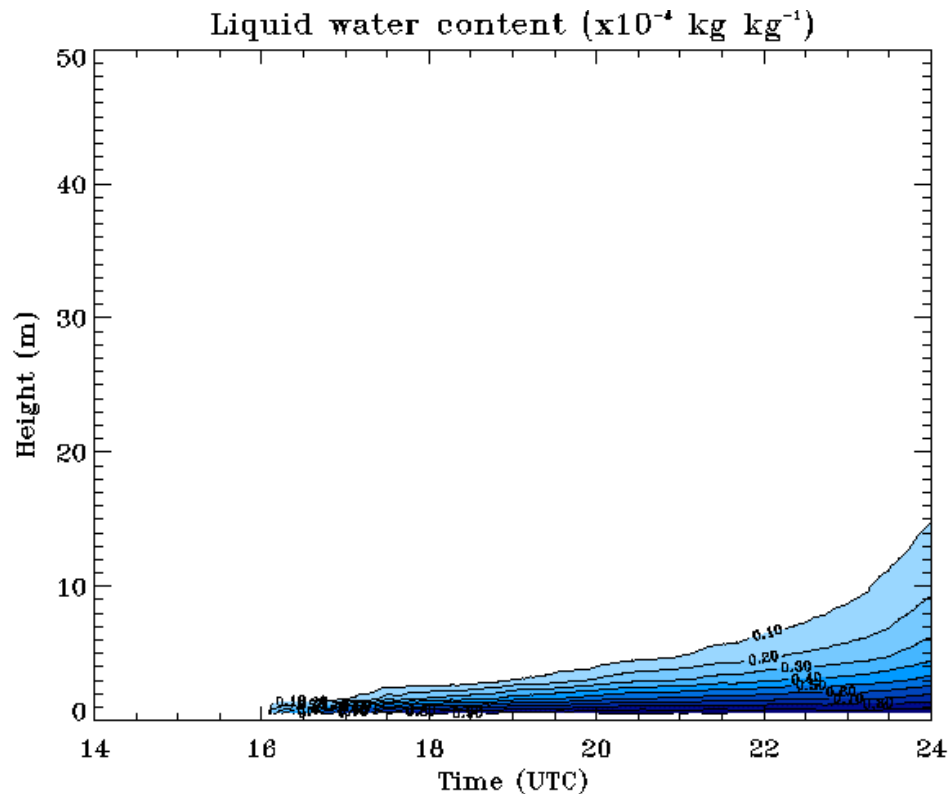


Fig. 7. Time-height cross-section of liquid water content for the simulation performed with $|V_g| = 4 \text{ ms}^{-1}$ without dew or frost deposition. Fog water content contours are shown at every 0.1 gkg^{-1} . The maximum water content shown is 0.8 gkg^{-1} .

Another simulation was performed while by considering that only *dewfall* occurs even is the surface temperature goes below the freezing point (“no frost” experiment). For the simulations performed, the skin surface temperature cools very rapidly after sunset and becomes lower than the freezing point slightly before 1600 UTC (Fig. 8). Results indicate the formation of a shallow ground fog layer forming a little after 1600 UTC and growing in the vertical starting at 2000 UTC (Fig. 9). The liquid water content is much lower than when dew/frost deposition is not taken into account, but nevertheless a fog layer forms during the evening, in opposition with the simulation performed with the dew/frost deposition parameterization.

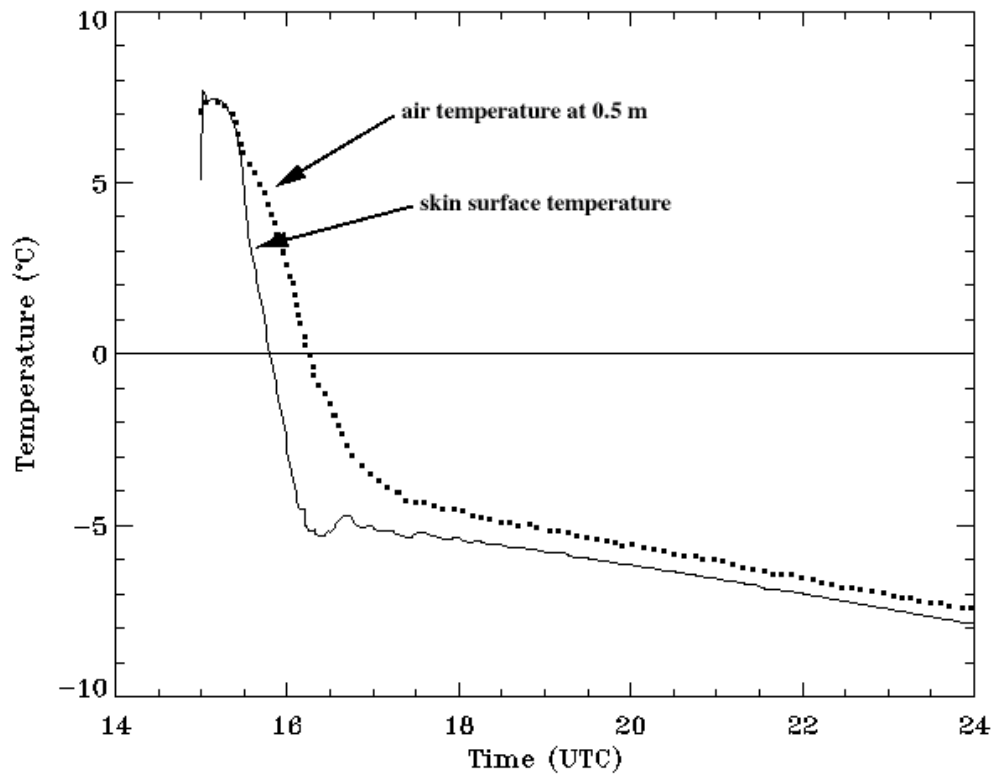


Fig. 8. Temporal evolution of the simulated skin surface temperature and the air temperature at the lowest model level for the simulation with $|V_g| = 4 \text{ ms}^{-1}$.

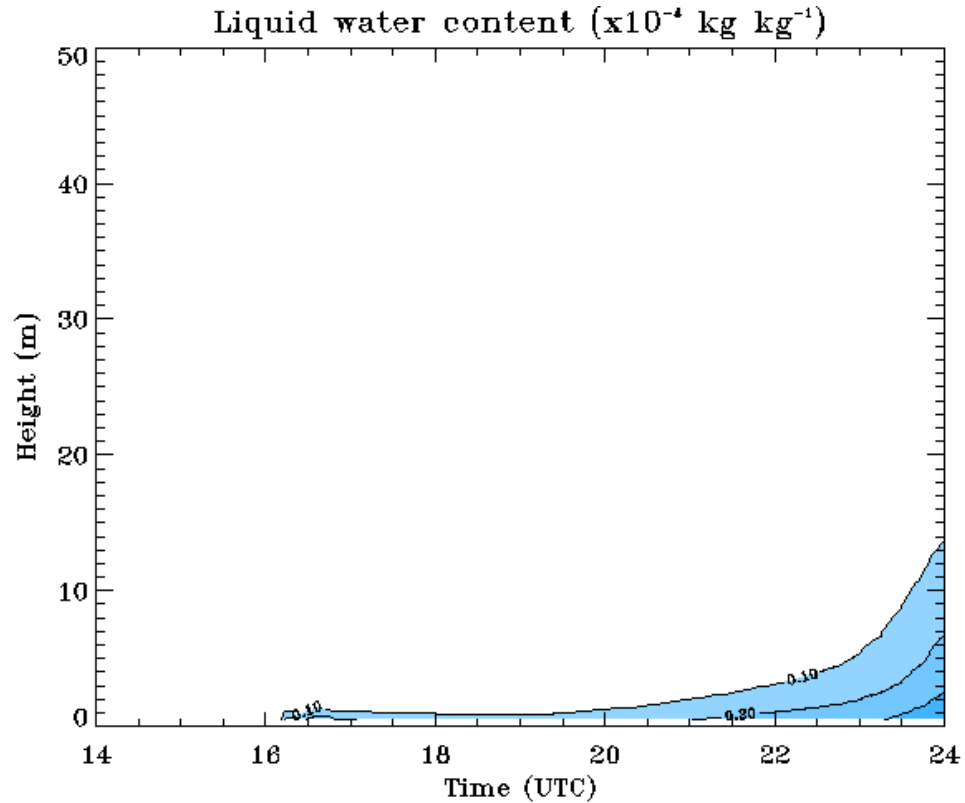


Fig. 9. Time-height cross-section of liquid water content for the simulation performed with $|V_g| = 4 \text{ ms}^{-1}$ with dew, but without frost deposition. Fog water content contours are shown at every 0.1 gkg^{-1} . The maximum water content shown is 0.3 gkg^{-1} .

Comparing the instantaneous water vapor flux to the surface obtained with and without considering the frost deposition (Fig. 10) shows the enhancement factor in the vapor flux related to the temperature dependence of saturation vapor pressure. When frost deposition is fully taken into account, the deposition of water vapor onto the surface is significantly larger from 1645 UTC onward. The enhancement factor of the vapor flux is by about 20% to 30%. This enhancement leads to more pronounced moisture depletion in the lower surface layer, enough to prevent the formation of a fog layer.

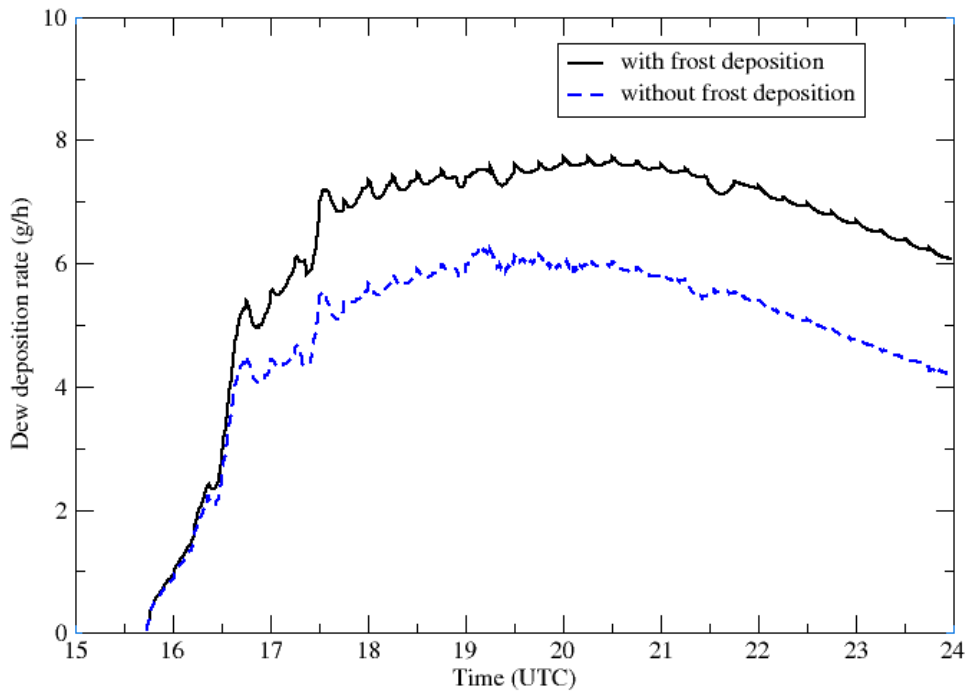


Fig. 10. Temporal evolution of the instantaneous rates of dew deposition obtained with and without considering the deposition of frost.

5. Summary and conclusions

A high-resolution boundary layer column (1D) model has been used to investigate the sensitivity and effect of dew deposition on fog layer onset over a bare homogeneous surface. Numerical experiments performed show significant sensitivity of dew deposition rates to specification of geostrophic wind speed (intensity of turbulence). The role of wind shear intensity (mixing) in a stable boundary layer is two-fold in its role of preventing the formation of fog layers: the entrainment of warm and dry air from above the inversion and the dehydration process in the lower part of the surface layer from the deposition of vapor to the surface as dew or frost.

The importance of dew/frost deposition on the formation of a fog layer was further illustrated with results from a “full physics” simulation compared to a simulation performed without the effect of dew/frost deposition. This shows that even if the water

vapor flux to the surface is not very large (a few grams per hour), it is nevertheless enough to control the formation of a fog layer. Also, the importance of frost deposition and its role in the enhancement of water vapor loss to the surface has been illustrated. Results suggest that supercooled fogs may be less likely to occur, compared to fogs forming in above freezing conditions.

These simple experiments using a comprehensive boundary layer fog model suggest the complexity, and thus difficulty, in modeling and forecasting the occurrence and variability of fog and its characteristics at the regional scale. Surface heterogeneities play an important role in determining the spatio-temporal distribution of the boundary layer structure (Acevedo and Fitzjarrald, 2001) and thus fog characteristics. This variability not only arises through the heat exchanges between the atmosphere and the surface (radiative and sensible heat fluxes) but also through the transfer of water between the surface and atmosphere. Subtle variations in surface properties can lead to significant differences in fog characteristics (depth, visibility). Fog being a “threshold phenomena”, regional scale to small scale variations in surface properties can also lead to differences in where and when a fog will form. This is one of the reasons why numerical mesoscale forecasting of fog at the regional scale has not been very successful so far. A complete description of the surface characteristics has to be combined with a high vertical resolution model to represent the small-scale gradients that are created in the nocturnal boundary layer. Comprehensive parameterizations of surface-atmosphere exchanges are also needed to account for the subtle processes taking place in the stable boundary layer.

Nevertheless, processes and interactions in the nocturnal boundary layer over complex terrain are still not completely understood. The small-scale advections related to different surface properties (footprint problem, interactions between drainage flows) are still not fully accounted for even in the most comprehensive existing models. Small-scale to mesoscale advections or moisture may offset the loss of atmospheric water vapor related to dew formation (Garratt and Segal, 1988) and thus play an important role in the formation of extensive fog layers at the regional scale. Nevertheless, progress in our understanding has been made over the last few years through field experiments and through modeling using Large Eddy Simulations. More research is needed in order to

better identify the role of these complex interactions in determining the formation of fog at the local and regional scales.

Appendix. Model description

a. General formulation

The COBEL model is based on dynamical and thermodynamical equations derived from the ensemble-average Boussinesq equations. Assuming horizontal homogeneity of momentum and of turbulent fluctuations but preserving a non-homogeneity in the large-scale temperature and humidity fields and including large-scale vertical motion, the resulting set of equations is:

$$\frac{\partial u}{\partial t} = f(v - v_g) - \frac{\partial}{\partial z}(\overline{w'u'}) - w \frac{\partial u}{\partial z}, \quad (\text{A.1})$$

$$\frac{\partial v}{\partial t} = -f(u - u_g) - \frac{\partial}{\partial z}(\overline{w'v'}) - w \frac{\partial v}{\partial z}, \quad (\text{A.2})$$

$$\frac{\partial \theta}{\partial t} = -\frac{\partial}{\partial z}(\overline{w'\theta'}) + \frac{\theta}{T} \left[-\frac{1}{\rho C_p} \frac{\partial F_r}{\partial z} + \frac{L}{C_p} C \right] - w \frac{\partial \theta}{\partial z} - \vec{V} \cdot \vec{\nabla} \theta, \quad (\text{A.3})$$

$$\frac{\partial q}{\partial t} = -\frac{\partial}{\partial z}(\overline{w'q'}) - C - w \frac{\partial q}{\partial z} - \vec{V} \cdot \vec{\nabla} q + E_r, \quad (\text{A.4})$$

$$\frac{\partial q_1}{\partial t} = -\frac{\partial}{\partial z}(\overline{w'q_1'}) + C + \frac{\partial G_c}{\partial z} - w \frac{\partial q_1}{\partial z} - P. \quad (\text{A.5})$$

The prognostic variables are: u and v , the zonal and meridional wind components respectively, θ , the potential temperature, q , the specific humidity and q_1 the liquid water content. In equations (A.1) and (A.2), the first term on the right-hand side ($f \cdot v$ or $-f \cdot u$) represents the Coriolis force while the second term represents the pressure force since the

geostrophic wind is related to the horizontal pressure gradient. The third term is the vertical divergence of turbulent fluxes of momentum while the last represents the vertical advection of momentum. The evolution of potential temperature (equation A.3) is determined by the vertical divergence of turbulent fluxes of heat (first term on the right), by the divergence of radiative fluxes (second term), by the release of latent heat when condensation occurs or by the evaporative cooling (third term) and by the vertical and horizontal advection of temperature (next to last and last terms on the right-hand side respectively).

The local specific humidity tendency (equation A.4) is governed by the vertical divergence of turbulent fluxes of water vapor, the condensation/evaporation rate of cloud water (C) as well as by the evaporation of rain (E_r) and finally by the vertical and horizontal advection of water vapor. It should be noted that term “ $L/C_p \cdot C$ ” of equation (A.3) does incorporate the diabatic effect of rainwater evaporation.

The evolution of cloud water content (equation A.5) is obtained by taking into account the turbulent transport of liquid water, condensation/evaporation, gravitational settling (sedimentation) of fog droplets and vertical advection. Term ‘ P ’ represents the conversion of cloud water into precipitation.

Horizontal visibility is evaluated using a relation proposed by Kunkel (1984) relating horizontal visibility to the liquid water content:

$$VIS(m) = \frac{3.9}{144.7(\rho q_l)^{0.88}} \cdot \quad (A.6)$$

In equations (A.1) and (A.2), the "g" subscript refers to the geostrophic wind components. It should be noted here that geostrophic wind components, horizontal advection of temperature and humidity and vertical motion are external parameters and can be calculated from the output of a mesoscale model or from analyses of observed data.

b. *Parameterizations*

1) RADIATIVE TRANSFER

The longwave radiation (4 to 100 μm) parameterization is a high-resolution spectral scheme with 232 spectral intervals between 4 and 100 μm (Vehil *et al.*, 1989). The net longwave radiative flux divergence is calculated at every model level by taking into account the emission and absorption by water (liquid and vapor), and CO_2 , as well as by the earth's surface. The transmission functions from Moskalenko (1968, 1969) and Golubitskiy and Moskalenko (1968) are used for the 4-22 μm spectral range, and those of Goody (1964) for the 22-100 μm range (Estournel *et al.*, 1983). The longwave optical depth is related linearly to the liquid water content as in Vehil *et al.* (1989).

Net shortwave radiation (0.24 to 4 μm) is computed at each model level using a version of the monospectral parameterization presented by Fouquart and Bonnel (1980). The radiative transfer is calculated while taking into account the scattering by water vapor, carbon dioxide, ozone and cloud droplets. Transmission functions for gaseous absorption are expressed in the form of Padé Approximants. The shortwave optical thickness is related to the liquid water content and an effective radius of cloud droplets, taken to be equal to 5 μm . The single scattering albedo of a cloud/fog layer is parameterized as a function of optical thickness. The scattering phase function's asymmetry factor is taken to be a constant (= 0.85).

2) TURBULENCE CLOSURE

The parameterization of turbulent fluxes is an extremely important aspect of one-dimensional modeling of the BL. Within COBEL, turbulent fluxes are parameterized using local K-theory:

$$\overline{w' \alpha'} = -K_{\alpha} \frac{\partial \alpha}{\partial z}, \quad (\text{A.7})$$

with $\alpha = m, \theta, q, q_1$. COBEL's turbulent closure scheme is a 1.5 order scheme (Stull, 1988, pp. 214-219). With such a closure scheme, the turbulent diffusion coefficients K_α are functions of stability dependent mixing lengths l_α and the turbulence kinetic energy (E_k) through:

$$K_\alpha = C_\alpha l_\alpha \sqrt{E_k}, \quad (\text{A.8})$$

where C_α is a constant equal to 0.4 (Peterson, 1969). The temporal evolution of the turbulence kinetic energy (TKE) is calculated through:

$$\frac{\partial E_k}{\partial t} = -\frac{\partial}{\partial z} \left(\overline{w'E'_k} + \frac{\overline{w'p'}}{\rho} \right) - \left(\overline{u'w'} \frac{\partial u}{\partial z} + \overline{v'w'} \frac{\partial v}{\partial z} \right) + \frac{g}{T} \overline{w'\theta'} - \varepsilon \quad (\text{A.9})$$

The first term on the right-hand side represents the turbulent transport of TKE, the second term represents the mechanical or shear production term, the third term represents the buoyant production or consumption and the last term represents dissipation of TKE. This expression is derived from the complete TKE budget equation by assuming horizontal homogeneity and by neglecting subsidence.

The turbulent transport/pressure-correlation term is obtained through the specification of a turbulent exchange coefficient:

$$\left(\overline{w'E'_k} + \frac{\overline{w'p'}}{\rho} \right) = -K_{E_k} \frac{\partial E_k}{\partial z} \quad (\text{A.10})$$

The K_{E_k} exchange coefficient is simply taken to be the average of adjacent K_m coefficients.

The dissipation term is specified following Delage (1974):

$$\varepsilon = \frac{a_\varepsilon C_\varepsilon}{l_\varepsilon} E_k^{1.5} \quad (\text{A.11})$$

where C_ε is equal to 0.064 and l_ε is the dissipation length. Term a_ε is obtained by assuming that the rate of production of TKE is nearly equal to that of viscous dissipation. This assumption is verified near the surface but an extension of its validity to the whole BL is only a presumption. a_ε is equal to 1.0 if only shear effects are considered, but becomes:

$$a_\varepsilon = \left(1 - \frac{l_\alpha}{kL_{mo}} \right) \quad (\text{A.12})$$

if the buoyancy term is considered. k is the von Karman constant and L_{mo} the local Monin-Obukhov length.

To complete the closure, mixing lengths l_m , l_θ , l_q , and l_{q1} , as well as the dissipation length, must be specified. COBEL incorporates four different mixing length formulations are used depending upon the static stability. Mixing lengths are specified for the stable regime, for the very stable regime, as well as for neutral conditions and for unstable stratification. For the stable and very stable regimes, mixing length relations are taken from Estournel and Guédalia (1987):

$$l_\alpha = l_\varepsilon = l_n (1 - 5 \cdot Ri) \quad \text{for } Ri < 0.16, \quad (\text{A.13})$$

$$l_\alpha = l_\varepsilon = l_n (1 + 41 \cdot Ri)^{-0.84} \quad \text{for } Ri > 0.16. \quad (\text{A.14})$$

In equations (A.13) and (A.14), $\alpha = m, \theta, q, q_1$ while Ri is the Richardson number and l_n is the mixing length for neutral conditions given by (Delage, 1974):

$$l_n = \frac{kz}{1 + kz/G} \quad (\text{A.15})$$

where $G = 4 \times 10^{-4} |\bar{V}_g| f^1$, f being the Coriolis parameter.

For the unstable regime, the formulation of Bougeault and Lacarrère (1989) is used:

$$l_\alpha = \min(L_{up}, L_{down}) \quad (\text{A.16})$$

$$l_\varepsilon = \sqrt{L_{up} \cdot L_{down}} \quad (\text{A.17})$$

where L_{up} and L_{down} are defined from:

$$\int_z^{z+L_{up}} \beta(\theta(z') - \theta(z)) dz' = E_k(z) \quad (\text{A.18})$$

$$\int_{z-L_{down}}^z \beta(\theta(z) - \theta(z')) dz' = E_k(z) \quad (\text{A.19})$$

L_{up} and L_{down} are upward and downward lengths defined as the distances that an air parcel can travel while using its kinetic energy to work against the buoyant force exerted on it by its environment. β is the buoyancy coefficient (g/T).

Stability is computed while taking into account the presence of liquid water when necessary. In the absence of liquid water, stability is diagnosed using the virtual potential temperature gradient:

$$\frac{d\theta_v}{dz} \begin{cases} < 0 \Rightarrow \text{unstable} \\ = 0 \Rightarrow \text{neutral} \\ > 0 \Rightarrow \text{stable} \end{cases} \quad (\text{A.20})$$

In the presence of liquid water, an expression derived from the formulation of the Brünt-Väisälä frequency of Durran and Klemp (1982) is used:

$$\left[\frac{T}{\theta} \frac{d\theta}{dz} + \Gamma_m - \frac{g}{c_p} \right] \left[1 + \frac{Lq_{sat}(T)}{RT} \right] - \frac{T}{1+q_w} \frac{dq_w}{dz} \begin{cases} < 0 \Rightarrow \text{unstable} \\ = 0 \Rightarrow \text{neutral} \\ > 0 \Rightarrow \text{stable} \end{cases} \quad (\text{A.21})$$

In equations (A.20) and (A.21), q_w is the total water specific humidity and Γ_m is the pseudo-adiabatic lapse rate which is given by (Triplet and Roche, 1977, p.64):

$$\Gamma_m = \Gamma_d \left[\frac{1 + \frac{Lq_{sat}}{R_d T}}{1 + \frac{q_{sat}}{C_{pa}} \left(C_{pv} + \frac{L^2}{R_v T^2} \left(1 + q_{sat} \frac{R_v}{R_d} \right) \right)} \right] \quad (\text{A.22})$$

where Γ_d is the dry adiabatic lapse rate, c_{pa} the specific heat at constant pressure of dry air and c_{pv} the specific heat at constant pressure of water vapor. R_d and R_v are the gas constants for dry air and water vapor respectively. Expressions (A.20) and (A.21) are also used in the computation of the Richardson number when evaluating mixing lengths.

3) MICROPHYSICS

As shown previously, the liquid water content (LWC) is a prognostic variable of the model. The scheme used is of the "bulk" type, meaning that only the total liquid water content is considered. The evolution of the droplet size distribution is not represented. Also, the solid phase is not considered in the model. Consequently, ice fogs cannot be simulated. If the temperature fall below the freezing point, only supercooled fogs are considered.

Cloud liquid water is produced (term 'C' in equation A.3) as soon as the specific humidity q becomes higher than the saturation specific humidity q_{sat} . The underlying assumption is that there is enough Cloud Condensation Nuclei (CCN) in the ambient air so that condensation occurs at low levels of supersaturation. Once the specific humidity becomes larger than its saturation value, the excess of water vapor condenses as liquid water (q_l). The equilibrium temperature T^* and specific humidity q^* are calculated by assuming conservation of energy and total water content. This translates into:

$$c_p T + Lq = c_p T^* + Lq^* , \quad (\text{A.23})$$

$$q^* = q_{\text{sat}}(T^*) , \quad (\text{A.24})$$

$$q + q_l = q^* + q_l^* . \quad (\text{A.25})$$

This set of equations is solved numerically using an iterative method. This approach is commonly referred to as "all or nothing" condensation. It assumes that an entire grid volume becomes saturated when specific humidity becomes larger than the saturation specific humidity. No subgrid-scale condensation scheme is used.

Gravitational settling of droplets is expressed following Brown and Roach (1976):

$$G_c = v_i q_l . \quad (\text{A.26})$$

This flux is only dependent on the liquid water mixing ratio (q_l) and a settling velocity v_i . This velocity is normally a function of the droplet size distribution. Since a "bulk" scheme is used here, this distribution is unknown. Nevertheless, an observational study has shown that droplets are small during the formation and dissipation phases, and that the shape of the droplet size spectra does not change noticeably during a fog layer's mature phase. Consequently, v_i is not expected to vary greatly during the lifetime of a fog layer (Guédalia and Bergot, 1992). The value used for v_i has been derived from observations of fog droplet size distributions and is taken to be 1.6 cm s^{-1} .

The precipitation (drizzle) parameterization is not described here since the precipitation module is switched off for the simulation of fog.

5) NUMERICAL ASPECTS

The model grid is composed of 30 levels distributed between the ground and an altitude of about 1.5 km using a log-linear function. Thus, resolution is highest in the lowest 100 m of the atmosphere. The lowest model level is at 0.50 m above the surface, the second is at 1.65 m and so on. The soil model uses 5 levels from the surface down to a depth of 1 m, the level closest to the surface being at 5 cm below the surface.

Five additional levels from 1.5 km to 5 km are used for radiative transfer computations. The atmospheric thermodynamic state is assumed to be in steady state for these levels.

The model equations are discretized using centered finite differences for spatial derivatives and time derivatives are forward in time. Fluxes are represented with an implicit formulation to ensure stability of the numerical solution. The time step is equal to 30 seconds.

References

- Acevedo, O. C. and D. R. Fitzjarrald, 2001: The early evening surface-layer transition: Temporal and spatial variability. *J. Atmos. Sci.*, **58**, 2650-2667.
- Bergot, T., 1993: *Modélisation du Brouillard à l'Aide d'un Modèle 1D Forcé par des Champs Mésoéchelle: Application à la Prévision*. Thèse de Doctorat, Université Paul Sabatier, Toulouse, France, No d'ordre 1546, 191p.
- Bergot, T., and D. Guédalia, 1994: Numerical forecasting of radiation fog. Part I: Numerical model and sensitivity tests. *Mon. Wea. Rev.*, **122**, 1218-1230.
- Bougeault, P., and P. Lacarrère, 1989: Parameterization of orography-induced turbulence in a meso-beta scale model.. *Mon. Wea. Rev.*, **117**, 1872-1890.
- Brown, R. and W. T. Roach, 1976: The physics of radiation fog, Part II: A numerical study. *Quart. J. Roy. Meteorol. Soc.*, **102**, 335-354.
- Delage, Y., 1974: A numerical study of the nocturnal boundary layer. *Quart. J. Roy. Meteor. Soc.*, **100**, 351-364.
- Durrán, D., and J. B. Klemp, 1982: On the effects of moisture on the Brunt-Väisälä frequency. *J. Atmos. Sci.*, **39**, 2152-2158.
- Estournel, C., R. Vehil, D. Guédalia, J. Fontan, and A. Druilhet, 1983: Observations and modeling of downward radiative fluxes (solar and infrared) in urban/rural areas. *J. Clim. Appl. Meteor.*, **22**, 134-142.
- Estournel, C., 1988: *Étude de la Phase Nocturne de la Couche Limite Atmosphérique*. Thèse de Doctorat d'État, Université Paul Sabatier, Toulouse, France, No. d'ordre 1361, 176p.
- Estournel, C., R. Vehil, D. Guédalia, J. Fontan, and A. Druilhet, 1983: Observations and modeling of downward radiative fluxes (solar and infrared) in urban/rural areas. *J. Clim. Appl. Meteor.*, **22**, 134-142.
- Estournel C., and D. Guédalia, 1987: A new parameterization of eddy diffusivities for nocturnal boundary layer modeling. *Bound. Lay. Meteor.*, **39**, 191-203.
- Fouquart, Y. and B. Bonnel, 1980: Computations of solar heating of the Earth's atmosphere: a new parameterization. *Beitrag zur Physik der Atmosphäre*, **53**, 35-62
- Garrat, J. R. and M. Segal, 1988: On the contribution of atmospheric moisture to dew formation. *Bound.-Layer Meteor.*, **45**, 209-236.

- Golubitskiy, B. M., and N. I. Moskalenko, 1968: Spectral transmission functions in the H₂O and CO₂ bands. *Atmos. Oceanic Phys.*, **4**, 194-203.
- Goody, R. M., 1964: *Atmospheric Radiation*. Oxford University Press, 436p.
- Guédalia, D. and T. Bergot, 1992: Premiers résultats de la campagne «Lille 88» d'étude du brouillard. *La Météorologie*, **42**, 11-20.
- Guédalia, D. and T. Bergot, 1994: Numerical forecasting of radiation fog. Part II: A comparison of model simulations with several observed fog events. *Mon. Wea. Rev.*, **122**, 1231-1246.
- Kunkel, B., 1984: Parameterization of droplet terminal velocity and extinction coefficient in fog model. *J. Appl. Meteor.*, **23**, 34-41.
- Lala, G. G., E. Mandel and J. E. Jiusto: 1975a: Numerical evaluation of radiation fog variables. *J. Atmos. Sci.*, **32**, 720-728.
- Lala, G. G., E. Mandel and J. E. Jiusto: 1975b: A numerical model of radiation fog, *Proceedings, Conference on Cloud Physics*, Tucson, Arizona, American Meteorological Society, 233-236.
- Mahrt, L. and H.-L. Pan, 1984: A two-layer model of soil hydrology. *Bound. Lay. Meteor.*, **29**, 1-20.
- Mihailovic, D. T., R. A. Pielke, B. Rajkovic, T. J. Lee and M. Jefic, 1993: A resistance representation of schemes for evaporation from bare and partly plant-covered surfaces for use in atmospheric models". *J. App. Meteor.*, **32**, 1038-1054.
- Monteith, J. L., 1957: Dew. *Quart. J. Roy. Meteorol. Soc.*, **83**, 322-341.
- Moskalenko, N. I., 1968: The spectral transmission function in some water-vapor bands and in the CO and CH₄ bands in the infrared. *Atmos. Oceanic Phys.*, **4**, 443-446.
- Moskalenko, N. I., 1969: The spectral transmission function in the bands of the water-vapor, O₃, N₂O and N₂ atmospheric components. *Atmos. Oceanic Phys.*, **5**, 678-685.
- Noilhan J., and S. Planton: A simple parameterization of land surface processes for meteorological models. *Mon. Wea. Rev.*, **117**, 536-549.
- Peterson, E. W., 1969: Modification of mean flow and turbulent energy by change in surface roughness under conditions of neutral stability. *Quart. J. Roy. Meteorol. Soc.*, **95**, 561-575.
- Peyraud, L., 2001: *Radiation Fog Forecasting Using a 1-d Model*. M.Sc. Thesis, University of Texas A&M, 82p.

- Pickering, K. E., and J. E. Jiusto, 1978: Observations of the relationship between dew and radiation fog. *J. Geophys. Res.*, **83**, 2430-2436.
- Pielke, R., 1984: *Mesoscale Meteorological Modeling*. Academic Press, Boston, 612 p.
- Pilié, R. J., E. J. Mack, W. C. Kocmond, W. J. Eadie and C. W. Rogers, 1975a: The life cycle of valley fog, Part I: Micrometeorological characteristics. *J. Appl. Meteor.*, **14**, 347-363.
- Pilié, R. J., E. J. Mack, W. C. Kocmond, W. J. Eadie and C. W. Rogers, 1975a: The life cycle of valley fog, Part II: Fog microphysics. *J. Appl. Meteor.*, **14**, 364-374.
- Stull, R. B., 1989: *An Introduction to Boundary Layer Meteorology*. Kluwer Academic Publishers, Boston, 666 p.
- Tardif, R., 2000: *The COBEL Model as a Stratus Burnoff Prediction Tool at SFO: Tests and Performance Evaluation Based on 1999 Cases*. Report presented to Massachusetts Institute of Technology Lincoln Laboratory, 24p.
- Triplet, J. P., and G. Roche, 1977: *Météorologie Générale*. 2nd edition, École Nationale de la Météorologie, Paris, 317p.
- Vehil, R., J. Monneris, D. Guédalia and P. Sarthou, 1989: Study of the radiative effects (long-wave and short-wave) within a fog layer. *Atmos. Res.*, **23**, 179-194
- Wattle, B. J., E. J. Mack, R. J. Pilié and J. T. Hanley, 1984: The role of vegetation in the low-level water budget in fog. In *FOG-82 – A Cooperative Field Study of Radiation Fog*. Atmospheric Sciences Research Center, State University of New York at Albany, Publication No. 984.